Symmetry breaking and structural changes at the neutral-to-ionic transition in tetrathiafulvalene-*p*-chloranil

M. Le Cointe, M. H. Lemée-Cailleau, H. Cailleau, B. Toudic, and L. Toupet
Groupe Matière Condensée et Matériaux, URA au CNRS 804, Université de Rennes 1, Bâtiment 11B, Campus de Beaulieu, 35042 Rennes Cedex, France

G. Heger,* F. Moussa, and P. Schweiss†
Laboratoire Léon Brillouin, Laboratoire Commun CEA-CNRS, CEN Saclay, 91191 Gif-Sur-Yvette Cedex, France

K. H. Kraft‡ and N. Karl
3. Physikalisches Institut, Universität Stuttgart, D-70550 Stuttgart, Germany
(Received 25 April 1994; revised manuscript received 11 October 1994)

The structural aspect of the temperature-induced neutral-to-ionic transition in the mixed-stack charge-transfer complex TTF-*p*-chloranil is directly analyzed using results obtained from neutron-scattering experiments. The symmetry breaking of the structural order parameter is determined together with the complete structural change. It is shown that the ionic phase is characterized by a dimerization along the stacking direction into weakly bond donor-acceptor dimers, which adopt a ferroelectric arrangement. Values of both dipole moment and dipolar energy in the unit cell are evaluated and commented. The evolution of the three-dimensional contacts which interconnect the chains, and in particular of the hydrogen interaction network, is discussed. Moreover, the associated intramolecular deformations are related in a satisfying way with the change of the ionicity and with the loss of centrosymmetry at the transition. Phenomena of metastability are also briefly discussed.

I. INTRODUCTION

Among the low-dimensional systems where electron-phonon interactions play a central role, the class of mixed-stack organic charge-transfer (CT) complexes which present the so-called neutral-to-ionic (N-I) phase transition is of greater current interest. Contrary to segregated-stack CT crystals giving rise to the well-known family of one-dimensional conductors, in these kinds of CT crystals which are always insulators or semiconductors, electron-donor (D) and electron-acceptor (A) molecules alternate along the same stack. These compounds can be classified into two categories according to the degree of CT ρ: quasi-neutral for $\rho<0.5$ and quasi-ionic for $\rho>0.5$. Several of them undergo a so-called neutral-to-ionic phase transition associated with a change of ionicity, i.e., of the degree of CT.[1-3] This uncommon electron-induced phase transition is observed generally at high pressure and only much more rarely at atmospheric pressure when it occurs at low temperature.[1-3]

Tetrathiafulvalene-*p*-chloranil (TTF-CA) is the prototypical example for this kind of phase transition, that can be obtained not only by an increase of pressure at room temperature, but also by simply lowering the temperature below $T_{N\text{-}I}\cong 80$ K at atmospheric pressure.[3] Since its discovery, in parallel to the development of many theoretical models,[4-10] the N-I transition in TTF-CA has been extensively studied by different spectroscopic techniques sensitive to electronic states. Thus, according to optical spectra, the degree of CT at atmospheric pressure is $\rho\cong 0.3$ in the N phase and $\rho\cong 0.7$ in the I phase.[11,12] Spectroscopic measurements[13,14] indicated the existence of a dimeric distortion in the I phase, in agreement with theoretical analyses.[7-10,15-17] In the same way, it has been shown that the transition at $T_{N\text{-}I}$ is clearly first order combined with some thermal hysteresis.[18-21] In addition, some pretransitional and precursor phenomena were observed recently by dielectric[22] and $^{35}C\ell$ nuclear quadrupolar resonance[21,23] (NQR) measurements. This NQR technique also yields information on local symmetry in relation to the breaking of inversion symmetry on the D and A molecules by the dimerization process. However, a direct study of these structural properties via diffraction techniques is requested for a complete description of the structural changes at the transition. Actually, although there are indications of a dimerization process in the I phase in literature, there is no information available about the symmetry breaking and the structural changes themselves, both essential to analyze in detail physical properties. Up to now, the crystal structure of the N phase was known at room temperature from an x-ray-diffraction analysis:[25] its space group is $P12_1/n1$ and the unit cell contains two equivalent nondimerized stacks with alternation of TTF and CA molecules located on inversion centers $(\frac{1}{2}\,\frac{1}{2}\,0)$ and $(0\,\frac{1}{2}\,0)$, respectively, (Fig. 1). There was also an attempt to study the dimerization process in the I phase by x-ray diffraction;[26,27] this analysis, however, was incomplete since only the $(2kl)$ and $(3kl)$ Bragg reflections were measured. In this way, the symmetry breaking at the transition could not be determined, since this requires a study of the systematic extinctions in the high-temperature phase, i.e., $h0l{:}h+l=2n+1$ and $0k0{:}k=2n+1$, and to follow their temperature evolu-

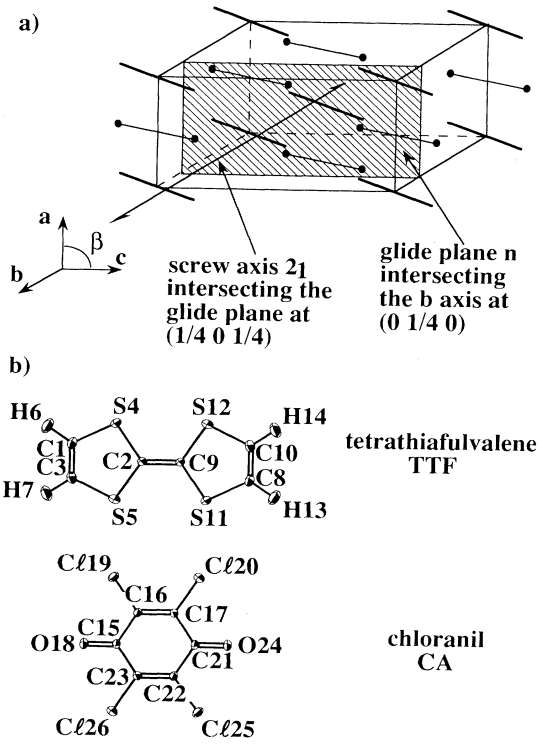

FIG. 1. (a) Schematic unit cell of TTF-CA in the high-temperature phase. The two different types of lines represent the long axes of the two types of molecules. (b) Molecules of TTF and CA with atom labeling.

tion. Furthermore, this first x-ray experiment did not allow to determine unambiguously the molecular displacements associated with the bond dimerization. Another important point is to know the change of the intramolecular geometry which is induced by the increase of the ionicity and the loss of inversion symmetry as suggested by a theoretical approach.[28] For these reasons we have undertaken, via accurate neutron-diffraction techniques, a direct and complete description of the structural aspects associated with the *N-I* phase transition in TTF-CA. The present paper is devoted to the analysis of the symmetry breaking and to a complete determination of the structural changes that are related to the instability. It will be followed by two others papers concerning the evolution of the transition under pressure, and hysteresis phenomena around $T_{N\text{-}I}$ with the occurrence of a plateau as observed from electric conductivity measurements,[19] in relation to the multipeak structure of the heat capacity.[24]

This paper is organized as follows. Section II presents a detailed study of the symmetry breaking. To improve resolution and signal-to-noise ratio, the experiments were performed on neutron triple-axis spectrometers. After this determination of the I space group, Sec. III presents the determination of the structural changes between the neutral and the ionic phases derived also from neutron-diffraction data, but collected on a four-circle diffractometer. Because neutron diffraction has the advantage to yield more reliable information on light elements than X-ray diffraction, it gave us a unique opportunity to carefully analyze the intramolecular and intermolecular changes with respect to the dimerization process, the ionicity change, and the modification of the interstack array, with special attention to C-H $\cdots$ O interactions. The latter may play a role in the transition in a similar way as in the halogen-bridged metallic compounds.[30] These aspects will be developed in Sec. IV.

II. SYMMETRY BREAKING AND CELL PARAMETER CHANGES AT THE *N-I* TRANSITION

A. Experiment

The study of symmetry breaking and cell-parameter changes was carried out by neutron scattering on the triple-axis spectrometers 4F1 and G4-3, installed on the cold source of the reactor Orphée at the Laboratoire Léon Brillouin (LLB). With these spectrometers we were able to detect weak Bragg reflections (of a selected equatorial plane of the reciprocal space) down to a level of about 10^{-4} of the strongest peak intensities. TTF-CA crystals were grown by the plate sublimation method in evacuated pyrex ampoules at a temperature of 76 °C of the lower and 74.5 °C of the upper plate. After freeing the upper plate from parasitic seeds by a short temperature increase to $\sim$80 °C and reequalization of the temperature profile, seeds were formed by a 5 to 8 °C supercooling step (maintained for a few minutes). Bulky, well-formed crystals up to $\sim$20 mm^3, grew in a few days.[31] The selected single crystal had the shape of a regular parallelepiped with dimensions $5\times3\times2$ mm^3. The cryogenic equipment used on these spectrometers allowed a temperature stability better than 0.02 K.

B. Results and discussion

The monoclinic symmetry $P12_1/n1$ of the high-temperature neutral phase[25] is responsible for two types of systematic extinctions: $0k0{:}k=2n+1$, because of the screw axis 2_1 parallel to **b** and $h0l{:}h+l=2n+1$ because of the glide plane n parallel to (**a**,**c**) (Fig. 1). Spectroscopic measurements,[13,14,21–23,32,33] indicating the loss of inversion symmetry associated with the formation of dimers, are in contradiction with the antiferroelectric order suggested for the ionic phase following dielectric measurements.[22] Actually, such an antiferroelectric arrangement would necessarily impose that the structure keeps some inversion center in the low-symmetry phase, possible only with a super cell, whose consequence would be the appearance of additional reflections at fractional indices along the main directions of the reciprocal lattice. On the other hand, a complete loss of inversion symmetry would involve the simultaneous loss of at least one of the two other symmetry elements, i.e., the screw axis 2_1 and/or the glide plane n, with the appearance of diffracted intensity on $0k0{:}k=2n+1$ and/or on $h0l{:}h+l=2n+1$. This would correspond to three possible space groups for the ionic phase, $P12_11$, $P1n1$ or

$P1$, all yielding a ferroelectric arrangement of the dimerized chains with an orientation of the dipole moment imposed by symmetry. To get such information about symmetry reduction, neutron-scattering measurements were performed on triple-axis spectrometers. The measurements were made in the scattering planes ($\mathbf{a}^*,\mathbf{b}^*$) and ($\mathbf{b}^*,\mathbf{c}^*$) to be able to study both types of systematic extinctions of the neutral phase and to look for superstructure reflections. During our investigations we got evidence that special care is required with handling the TTF-CA crystal because they are particularly sensitive to external conditions such as stress, that can even be introduced by their fixing. As a result, metastable phenomena[20] may occur which will be discussed later. Under reversible conditions, we found no superstructure reflections at fractional indices along the main directions of the reciprocal lattice, thus an antiferroelectric arrangement can be disregarded. The structural transition is then translation equivalent and takes place at the center of the Brillouin zone. On the other hand, only the $(0k0)$ reflections with $k=2n+1$ appear below $T_{N\text{-}I}\cong 81.7$ K with a significant intensity and a Bragg profile typical of long-range order, while the $(h0l)$ reflections with $h+l=2n+1$ remain systematically absent in the ionic phase (Fig. 2). These features imply the lack of the twofold screw axis 2_1 but the persistence of the glide plane n in the low temperature phase. Thus the space group of the ionic phase is $P1n1$ with a ferroelectric arrangement of two equivalent dimerized stacks and a dipole moment lying in the ($\mathbf{a},\mathbf{c}$) plane. The structural order parameter is therefore of B_u symmetry, according to the point-group symmetry C_{2h} [Fig. 2(c)] and is an admixture of the dimerization and the related intramolecular deformation.

Besides these findings, the cell parameters shown in Fig. 3 give also some clear structural evidence of the phase transition. On the one hand, the strong contraction of the stacking axis **a** with decreasing temperature in the neutral phase is confirmed.[3] The phase transition temperature $T_{N\text{-}I}$ is then indicated by a simple change of the slope, as the contraction is noticeably reduced in the ionic phase. On the other hand, although the transition is nonferroelastic, the **b** and **c** cell parameters present an abrupt jump at $T_{N\text{-}I}$ which is much more pronounced for $\Delta b/b\cong 0.5\%$ than for $\Delta c/c\cong 0.1\%$. This behavior strongly evidences the three-dimensional nature of the interactions, as well as the quite important volume variation at $T_{N\text{-}I}$, both being generally not considered in literature. These structural aspects will turn out to be of fundamental importance for the interpretation of pressure effects or metastability.

We now want to describe the metastable phenomena observed with TTF-CA crystals stressed via sticking or thermal constraint induced by cooling.[20] With freshly sticked samples, it was possible to evidence in the high-temperature phase, that the symmetry forbidden reflections $0\,k\,0{:}k=2n+1$ and $h\,0\,l{:}h+l=2n+1$ were present. Their very weak intensities detectable only thanks to the high sensitivity of the triple-axes spectrometers used, relaxed to zero after a few weeks. Moreover, contrary to ordinary Bragg peaks such as (200) or (002), $(h0l)$ reflections with $h+l=2n+1$ were abnormally broadened along $\mathbf{a}^*$ or $\mathbf{c}^*$ (their width was more than three times the expected value). Thus they are not characteristic for a long-range order. On lowering temperature, the intensity of these reflections sharply increased at the phase transition but then did not return to the previous value when back at high temperatures. This is another evidence of metastable behavior. A rapid cooling with a fast crossing of the transition created a similar

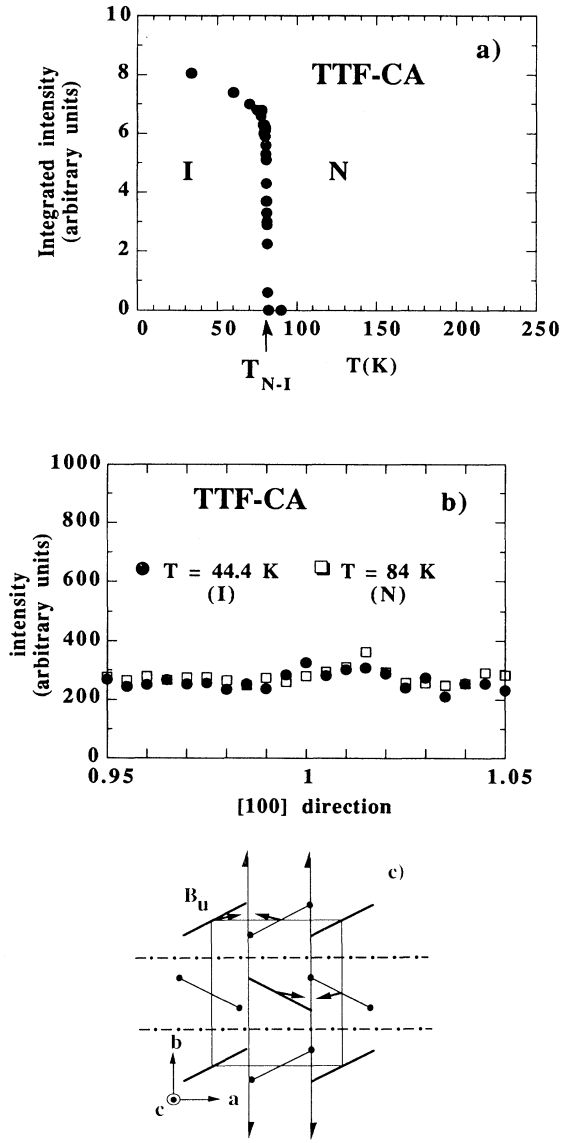

FIG. 2. (a) Evolution with temperature of the integrated intensity of the characteristic reflection (0 3 0). Error bars are smaller than the diameter of the symbols indicating the quality of the data. (4F-1 LLB, atmospheric pressure, decreasing temperature, $k_i=1.54$ Å^{-1} collimations 40′/40′, Be filter). (b) Longitudinal scan of the (100) reflection in both phases. (4F-1 LLB, atmospheric pressure, $k_i=1.54$ Å^{-1} collimations 40′/40′, Be filter). (c) Schematic drawing of an example of the critical ferroelectric B_u mode.

appearance of forbidden reflections in the high-temperature phase after reheating, starting from the proper $P12_1/n1$ state. This peculiar behavior of characteristic reflections does not seem to be directly related to the neutral-to-ionic instability and might be interpreted as the response of the material to some internal or external stresses (probably B_g symmetry shear) or as the diffraction by domain-wall areas.

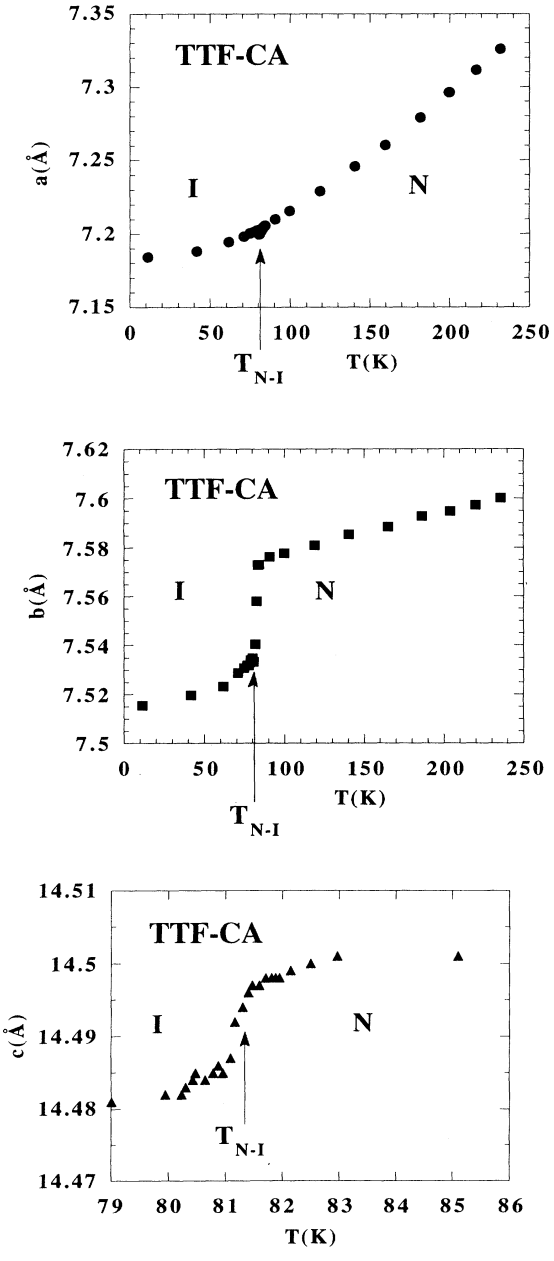

FIG. 3. Evolution with temperature of the cell parameters **a**, **b**, and **c**. (G4-3 LLB, atmospheric pressure, increasing temperature, $k_i = 1.5$ Å^{-1} for **a** and **b**, $k_i = 1.1$ Å^{-1} for **c**, collimations 30′/30′, Be filter).

III. CHANGES OF THE CRYSTAL STRUCTURE BETWEEN THE NEUTRAL AND THE IONIC PHASES

A. Experiment

A crystal structure determination was carried out by neutron diffraction on the four-circle diffractometer 5C2, installed on the hot source of the reactor Orphée at the LLB. A focusing Cu (2 2 0) monochromator [$\lambda = 0.831(1)$ Å] was used, associated with an erbium filter in order to eliminate $\lambda/2$ contamination [remaining $I(\lambda/2) \approx 0.1\%$]. Horizontal and vertical divergences were 57′ and 3°, respectively. To avoid any peak overlap that might have been caused by the poor vertical resolution, the **c** axis with its largest cell parameter was set perpendicular to the ϕ axis. The helium gas-flow cryostat (Oxford Instruments) used for measurements in the N and I phases (300, 90, and 40 K) on this diffractometer allowed data collections with a temperature stability of ±0.5 K. Data collections were performed on a nontwinned and nonstressed crystal of prismatic shape ($1.4 \times 5.0 \times 1.8$ mm^3), grown by the plate sublimation method described above. Thirty reflections were chosen in all reciprocal space for the determination of the orientation matrices and the unit-cell parameters [at 300 K: **a** = 7.40(1), **b** = 7.620(8), **c** = 14.59(2), $\beta = 99.1(1)°$; at 90 K; **a** = 7.22(2), **b** = 7.59(2), **c** = 14.49(4), $\beta = 99.1(2)°$; at 40 K: **a** = 7.19(3), **b** = 7.54(2), **c** = 14.44(4), $\beta = 98.6(3)°$]. Multiple scattering was verified to be negligible. The scanning procedure $\omega/2\theta$ was adopted for $3° \le 2\theta \le 75°$, corresponding to a reciprocal-space section according to h: −11 to +11, k: −11 to +11, l: −21 to 0 at 300 K, or h: 0 to 11, k: −11 to +11, l: −21 to +21 at 90 and 40 K. Standard reflections [(210) and $(00\bar{8})$ at 300 K, (210), (029), and $(20\bar{2})$ at 90 and 40 K], repeated every 300 min, assured a stability of measurements better than 1%. Absorption and Lorentz factor corrections were carried out.

B. Structures of the neutral and the ionic phases

1. Neutral phase

Diffraction data were collected at 300 and 90 K. Taking into account the observation of pretransitional phenomena,[21–23,34] the most appropriate conditions were chosen to get information on the thermal evolution of the atomic positions of the TTF and CA molecules, especially along the stacking axis which is the direction that is the most sensitive to temperature variation in the high-symmetry phase.[29] It was first verified that the symmetry forbidden reflections in the neutral phase ($0k0: k = 2n+1$ and $h0l: h+l = 2n+1$) were absent. Then, the structure was refined with space group $P12_1/n1$, $Z = 2$, by a least-squares minimization of $w(|F_0| - |F_c|)^2$. At convergence, the final residuals[35] were $R = 3.5$ and 3.4% and $R_w = 2.7$ and 2.3% at 300 and 90 K, respectively, for 1118 and 1223 independent reflections with $F_0 > 2.5\sigma(F_0)$, 118 parameters (atomic coordinates, anisotropic temperature factors, and scale factor); the goodness of fit[35] were 1.46 and 1.40, respectively. The final atomic parameters are listed in Table I.

TABLE I. Fractional atomic coordinates ($\times 10^4$) and anisotropic thermal motion parameters ($\times 10^4$) with standard deviations in parentheses. The temperature factors U_{ij} are given in the form $\exp[-2\pi^2(U_{11}h^2a^{*2}+U_{22}k^2b^{*2}+U_{33}l^2c^{*2}+2U_{12}hka^*b^*+2U_{13}hla^*c^*+2U_{23}klb^*c^*)]$; $U_{eq}=\frac{1}{3}(U_{11}+U_{22}+U_{33}+2\cos\beta U_{13})$ ($\times 10^4$) (Å^2); $B_{eq}=8\pi^2U_{eq}$ (Å^2).

Atom	x/a	y/b	z/c	U_{11}	U_{22}	U_{33}	U_{12}	U_{13}	U_{23}	U_{eq}	B_{eq}
					$T=300$ K						
C1	3131(2)	1465(2)	−940(1)	396(8)	278(7)	505(9)	−44(7)	112(7)	−86(8)	381	3.00
C2	4627(2)	4338(2)	−283(1)	324(6)	236(7)	286(6)	−12(6)	51(5)	16(6)	277	2.19
C3	3369(2)	2409(2)	−1680(1)	383(8)	405(9)	390(8)	1(7)	69(6)	−124(8)	385	3.04
S4	3866(5)	2379(5)	142(2)	39(2)	26(2)	37(2)	−4(1)	8(1)	4(1)	333	2.63
S5	4394(5)	4450(6)	−1494(2)	39(2)	45(2)	27(1)	3(2)	7(1)	3(1)	363	2.87
H6	2499(6)	161(5)	−952(3)	83(3)	40(2)	90(3)	−22(2)	21(2)	−13(2)	688	5.43
H7	2985(6)	1992(6)	−2400(3)	85(3)	75(3)	48(2)	−7(2)	8(2)	−27(2)	687	5.42
C15	407(2)	6400(2)	−614(1)	331(6)	277(7)	282(6)	5(6)	90(5)	−63(6)	287	2.27
C16	−448(2)	4730(2)	−986(1)	297(6)	314(7)	249(6)	16(6)	52(5)	−46(5)	281	2.22
C17	−788(2)	3416(2)	−414(1)	279(6)	255(7)	290(6)	27(5)	61(5)	−25(6)	268	2.12
O18	824(3)	7540(3)	−1123(1)	62(1)	347(9)	363(9)	87(9)	155(8)	−100(8)	425	3.35
Cℓ19	−892(2)	4553(2)	−2161(1)	485(6)	606(8)	254(5)	92(6)	38(4)	−46(5)	445	3.51
Cℓ20	−1661(2)	1457(2)	−822(1)	451(6)	326(5)	453(6)	88(5)	63(5)	34(5)	404	3.19
					$T=90$ K						
C1	3097(2)	1418(2)	−933(1)	105(6)	80(5)	136(5)	−22(5)	19(4)	−24(5)	105	0.83
C2	4621(2)	4327(1)	−284(1)	137(7)	61(5)	87(5)	−19(5)	21(4)	−1(5)	93	0.73
C3	3356(2)	2361(2)	−1685(1)	123(7)	108(6)	113(5)	−5(4)	25(4)	−31(4)	112	0.88
S4	3857(4)	2365(4)	164(2)	12(1)	9(1)	12(1)	0(1)	1(1)	1(1)	108	0.85
S5	4425(4)	4417(4)	−1502(2)	10(1)	10(1)	10(1)	1(1)	22(9)	2(1)	98	0.77
H6	2463(5)	128(4)	−950(2)	34(2)	17(1)	34(1)	−10(1)	8(1)	−3(1)	276	2.18
H7	2978(5)	1948(4)	−2405(2)	35(2)	33(1)	20(1)	−3(1)	3(1)	−8(1)	290	2.29
C15	445(2)	6391(2)	−626(1)	112(6)	78(5)	89(4)	8(5)	30(4)	−17(4)	90	0.71
C16	−436(2)	4716(2)	−989(1)	100(6)	89(5)	79(5)	13(5)	14(4)	−12(4)	88	0.69
C17	−800(2)	3401(2)	−407(1)	101(6)	71(5)	81(4)	5(4)	23(4)	−8(4)	82	0.65
O18	899(2)	7523(2)	−1144(1)	193(8)	96(6)	116(6)	33(5)	43(5)	−25(5)	130	1.03
Cℓ19	−870(1)	4500(1)	−2178(1)	135(5)	151(4)	70(3)	25(3)	8(3)	−10(3)	118	0.93
Cℓ20	−1694(1)	1424(1)	−819(1)	121(5)	80(3)	129(4)	25(3)	15(3)	7(3)	108	0.85

2. *Ionic phase*

The data collection was carried out at 40 K, i.e., in a temperature range of the ionic phase where the order parameter is saturated. Consequently, a maximal structural difference could be expected. In spite of a counting time three times larger than for the fundamental Bragg peaks, only the (0 7 0) superstructure reflection was clearly extracted from the background. All (h 0 l) reflections with $h+l=2n+1$ remained absent as expected from the analysis of space-group symmetry. The same procedure of refinement as described above was applied but with the space group $P1n1$, $Z=2$, using 1636 independent reflections [$F_0>2.5\sigma(F_0)$] for 105 parameters (atomic coordinates, isotropic thermal factors and scale factor). Because of the doubling of the number of independent atoms in the unit cell, only isotropic thermal parameters could be refined. The reliability factors[35] were $R=5.0\%$ and $R_w=3.8\%$ with a goodness of fit[35] equal to 1.48. Like in the neutral phase, these numbers illustrate the quality of the structure determinations. Final atomic parameters are given in Table II. One should notice that the standard deviations have very small values.

IV. DISCUSSION

A. Dimerization and intermolecular displacements

The structural deformation in the ionic phase, compared to the neutral one, takes mainly place in the dimerization, i.e., the formation of singlet (TTF-CA) pairs along the stacking axis **a**: molecular centers are shifted (Table III) and, instead of the single D-A distance $d=3.70(1)$ Å observed in the high-symmetry phase, two distinct D-A distances, $d_{intra}=3.504(4)$ Å and $d_{inter}=3.685(4)$ Å, alternate now along the stacking direction. The created dipole moments adopt a ferroelectric array. We think that this ferroelectric arrangement of dimers in the ionic phase should be closely related to the large increase of the dielectric susceptibility observed in the neutral phase closed to $T_{N\text{-}I}$.[22] Assuming that the partial charge ($\rho\cong 0.7$[11]) transferred from D to A in the ionic phase is located on the new molecular center positions, a dipole moment μ of 0.6(1) Debye per unit cell, lying in the (**a**,**c**) plane, can be calculated. Notice that this evaluation is a relatively rough one since it does not take into account the noncentrosymmetry of the π electron

TABLE II. Fractional atomic coordinates ($\times 10^4$) and isotropic thermal motion parameters (Å^2) at 40 K. Standard deviations are given in parentheses. In order to keep the choice of the unit cell of the high-temperature structure, the glide plane is at $y = \frac{1}{4}$.

Atom	x/a	y/b	z/c	B_{eq}	Atom	x/a	y/b	z/c	B_{eq}
C1	3099	1418(1)	−938	0.39(1)	C8	6909(1)	8603(1)	936(1)	0.73(1)
C2	4497(1)	4368(1)	−281(1)	0.37(1)	C9	5259(1)	5739(1)	298(1)	0.41(1)
C3	3398(1)	2360(1)	−1674(1)	0.70(1)	C10	6664(1)	7634(1)	1706(1)	0.44(1)
S4	3751(3)	2395(3)	176(1)	0.51(2)	S11	6090(3)	7658(3)	−135(1)	0.43(2)
S5	4427(3)	4471(3)	−1496(1)	0.34(2)	S12	5555(3)	5621(3)	1508(1)	0.52(3)
H6	2436(3)	124(2)	−983(1)	1.32(3)	H13	7563(3)	9933(3)	917(1)	1.74(3)
H7	3113(2)	1971(2)	−2416(1)	1.12(2)	H14	7105(3)	8067(3)	2416(2)	2.41(4)
C15	642(1)	6373(1)	−591(1)	0.49(1)	C21	−335(1)	3585(1)	674(1)	0.40(1)
C16	−265(1)	4691(1)	−947(1)	0.49(1)	C22	558(1)	5259(1)	1027(1)	0.32(1)
C17	−673(1)	3393(1)	−364(1)	0.55(1)	C23	948(1)	6581(1)	429(1)	0.30(1)
O18	1125(1)	7500(1)	−1124(1)	0.60(1)	O24	−819(1)	2432(1)	1196(1)	0.56(1)
Cℓ19	−796(1)	4517(1)	−2148(1)	0.37(1)	Cℓ25	883(1)	5549(1)	2211(1)	0.70(1)
Cℓ20	−1649(1)	1427(1)	−783(1)	0.51(1)	Cℓ26	1785(1)	8596(1)	855(1)	0.46(1)

distribution. The dipolar energy W_d can then be estimated according to $W_d \cong \mu^2/4\pi\varepsilon_0 V$, where V is the volume occupied by the dipole moment μ.[36] This estimate is negligible in comparison to $k_B T_{N\text{-}I}$, ($W_d/k_B \cong 3$ K), so that long-range dipolar interactions would not be able to be the driving force for the N-I transition. Furthermore, the displacement values (Table III) explain the encountered difficulties when studying the symmetry breaking. Actually, if the dimerization is characterized mainly by a displacement of the molecules along the stacking axis **a**, the intensity of the reflections $0k0{:}k = 2n + 1$, is sensitive to the atomic displacement along the **b** direction, which is very small.

Among intermolecular distances in the dimer (TTF-CA), 15 exhibit an abnormal temperature behavior with respect to the minimal sum of the van der Waals radii[37] of the implicated atoms as illustrated in Fig. 4 and Table IV. The column indexed TC gives estimated distances when only the thermal contraction of the lattice is considered, i.e., when the intramolecular geometry and the global molecular orientations are taken to remain constant. At $T_{N\text{-}I}$, the **b** and **c** parameters exhibit a jump while the **a** parameter shows only a change of its contraction (Ref. 20 and Fig. 3). Therefore, the **b** and **c** parameters used for the estimate at 40 K (column TC) were taken larger than the observed ones by the amount of the jump at the transition, i.e., as they should be if there was no transition. In the neutral phase, only few distances (2 at 300 K and 7 at 90 K) were already found too small with respect to the normal van der Waals radii without any very significant discrepancy compared to the x-ray results.[25] This increase of the number of such pathological contacts in the neutral phase could be predicted already by the simple thermal contraction. This feature can also be related to the effect of the weakly increasing partial charge transfer in the high-temperature phase.[11] Below $T_{N\text{-}I}$, a collective dimerization process is clearly evidenced, leading to the formation of singlet (D-A) pairs giving rise to the diamagnetic state of the ionic phase. Along the stacking axis, there are now clearly two

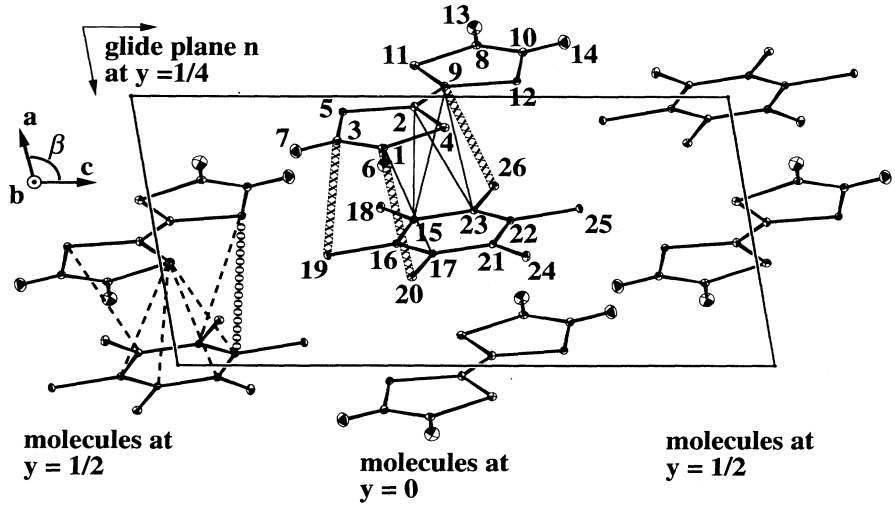

FIG. 4. Projection onto the (**a**,**c**) plane of C-C (——), C-Cℓ (XXXX), S-C (— — —), and S-Cℓ (OOOO) distances shorter than the sum of van der Waals radii at 40 K. For clarity, these distances are drawn on two equivalent dimers.

TABLE III. Molecular center displacements (Å) at 40 K, compared to the neutral phase, and the corresponding dipole moment (Debye) along the crystallographic axes **a**, **b**, and **c**. Standard deviations are given in parentheses.

	a	b	c
Displacements (Å):			
TTF	−0.007(1)	0.019(1)	0.0035(6)
CA	0.0842(6)	−0.0061(6)	0.0523(3)
Dipole moment (Debye):			
In the chain	−0.30(6)	−0.09(3)	−0.15(3)
In the unit cell	−0.6(1)	0.00(6)	−0.30(6)

distinct distances between the TTF and CA molecules which were identical by inversion symmetry in the neutral phase. The longest intermolecular distances at 40 K are characteristic of normal van der Waals interactions. The shortest ones, which can in no case be explained simply by the thermal contraction, have to be related to the dimerization process (except for C3-Cℓ19). Let us note that the intermolecular bondings connect essentially one-half of the TTF with the whole CA molecule. Such an asymmetry between the two cycles of the TTF molecule can also be observed in the evolution of the dihedral angle between the least-squares planes of the TTF and the CA molecules: the TTF cycle formed of atoms labeled 1–7 gets closer to the electron-acceptor molecule, with its mean plane more parallel to the CA plane. These features are further discussed in Sec. IV C in their relation to molecular deformations and bond dimerization.

B. Interstack arrays

The physical properties of the TTF-CA crystal were interpreted in the literature according to its obvious one-dimensional character. However it is essential to keep in mind the three-dimensional aspects of the system, in particular to elucidate the features that TTF-CA displays in the other directions (e.g., the drastic jumps of the **b** and **c** parameters at $T_{N\text{-}I}$, Fig. 3). Structure analyses in both the neutral and the ionic phase give the opportunity to examine precisely the interstack molecular rearrange-

TABLE IV. Evolution of typical intermolecular distances. Distances shorter than the sum of van der Waals radii are marked by an asterisk *. Symmetry equivalent distances in the high-temperature phase are given in curly brackets.

		X rays (Ref. 23)	Neutrons, this work					
		300 K	300 K	90 K_{TC}	90 K	40 K_{TC}	40 K	
				Inside the chain				
							shorter distances	longer distances
C-C (Å)								
	C1-C17	3.448	3.452(2)	3.378(5)*	3.386(2)*	3.360(5)*	3.306(1)*	3.454(1)
	C2-C15	3.467	3.461(2)	3.386(5)*	3.368(2)*	3.369(5)*	3.130(1)*	3.529(1)
	C2-C23	3.607	3.599(2)	3.528(5)	3.533(2)	3.511(5)	3.336(1)*	3.665(1)
	C9-C15	3.737	3.744(2)	3.665(5)	3.643(2)	3.646(5)	3.409(1)*	3.811(1)
	C9-C23	3.508	3.500(2)	3.417(5)	3.416(2)	3.397(5)*	3.197(1)*	3.569(1)
C-Cℓ (Å)								
	C1-Cℓ20	3.583	3.578(2)	3.492(5)*	3.494(2)*	3.472(5)*	3.454(1)*	3.525(1)
	C3-Cℓ19	3.525	3.523(2)	3.449(5)*	3.434(2)*	3.431(5)*	3.404(1)*	3.397(1)*
	C9-Cℓ26	3.699	3.697(2)	3.631(5)	3.634(1)	3.616(5)	3.482(1)*	3.704(1)
S-C (Å)								
	S4-C17	3.499	3.502(4)*	3.421(7)*	3.429(3)*	3.402(7)*	3.248(2)*	3.560(2)
	S4-C21	3.470	3.469(4)*	3.338(7)*	3.416(3)*	3.369(7)*	3.253(2)*	3.568(2)
	S4-C16	3.794	3.802(4)	3.736(7)	3.737(3)	3.720(7)	3.545(2)*	3.847(2)
	S4-C22	3.712	3.709(4)	3.647(7)	3.659(3)	3.632(7)	3.505(2)*	3.764(2)
	S5-C15	3.719	3.710(4)	3.638(7)	3.646(3)	3.620(7)	3.498(2)*	3.688(2)
	S12-C23	3.750	3.748(4)	3.672(7)	3.647(3)	3.654(7)	3.519(2)*	3.744(2)
S-Cℓ (Å)								
	S12-Cℓ26	3.709	3.713(4)	3.649(8)	3.624(3)*	3.634(8)*	3.536(2)*	3.663(2)
				Between the chains				
Cℓ-Cℓ (Å)								
	Cℓ-Cℓ(1)	{3.508}*	{3.517(2)}*	{3.437(4)}*	{3.470(2)}*	{3.421(4)}*	3.444(1)*	
	Cℓ-Cℓ(2)						3.496(1)*	
C-Cℓ (Å)								
	C-Cℓ(1)	{3.482}	{3.476(2)}*	{3.436(5)}*	{3.418(2)}*	{3.428(5)}*	3.371(1)*	
	C-Cℓ(2)						3.384(1)*	
S-Cℓ (Å)								
	S-Cℓ(1)	{3.567}	{3.564(4)}*	{3.497(7)}*	{3.477(3)}*	{3.479(7)}*	3.403(2)*	
	S-Cℓ(2)						3.471(2)*	

ment that occurs in conjunction with the dimerization process. In this way, a systematic comparison of atom distances with the corresponding sum of van der Waals radii reveals several types of too-close contacts. Let us consider first the few which are repulsive for electrostatic reasons; they concern chlorine atoms of the CA molecules belonging to different stacks (Fig. 5, Table IV) and generate planes of Cℓ-Cℓ contacts parallel to the $(1\,0\,\bar{1})$ lattice plane. Cℓ-Cℓ distances determined between 300 and 40 K show that this repulsive interaction is already quite important at room temperature. A main feature of the phase transition is to stop the decrease of the Cℓ-Cℓ distance by reorientation of CA molecules; these distances would become too short at 40 K with respect to Coulomb interactions if only thermal contraction would occur. On the other hand, most of the other too-close contacts can be easily understood in terms of attractive electrostatic forces. They implicate sulfur and external carbon atoms of the TTF molecules and once more the chlorine atoms of the CA (Table IV). These interactions link molecules belonging to different stacks. C-Cℓ contacts define chains almost parallel to the long axis of TTF, along the $[0\,1\,\bar{1}]$ direction for molecules in the basic plane and along $[0\,1\,1]$ for molecules located at $x=\frac{1}{2}$ (Fig. 6). The chains defined in this way are connected to each other by the S-Cℓ contacts, as shown in Fig. 7, forming strongly intermeshed planes. At 90 K, thermal contraction alone is hardly sufficient to explain the experimental distances. As already discussed for the one-dimensional intrastack geometry, this could be related to the slight increase of the degree of molecular ionicity that also favors attractive Coulomb interactions in three dimensions. Thus, because at 40 K the charge-transfer between *D* and *A* molecules and consequently Coulomb interactions become more significant, the experimental values clearly differ from those expected simply by thermal contraction effects. This behavior underlines sharply the great importance of the interstack interactions for the neutral-to-ionic phase transition. All these contacts, including the hydrogen bonds discussed below, are involved in bringing chains closer to each other in the ionic phase, and it is not possible to extract one particular interaction which alone could explain the anomalies observed for the **b** and **c** parameters across $T_{N\text{-}I}$.

From x-ray structure analysis of Ref. 25, Batail *et al.*[29] qualitatively reported on an existence of a network of C-H $\cdots$ O intermolecular contacts in TTF-CA. Such interactions were considered as efficient in the packing of molecular crystals,[38–40] in particular for "compounds containing atoms of varying electronegativities, with, frequently, a conjugated double-bond system or a series of double bonds."[41] TTF-CA is a good candidate for investigating such a behavior since its neutral-to-ionic transition modifies the electronic distribution. Our structural study by neutron diffraction on both sides of the transition also allowed us to determine the H-bonding distances very accurately (in contrast to x-ray diffraction), and to elucidate their part in the structural distortion. Two different kinds of C-H $\cdots$ O interactions exist (Table V and Figs. 6 and 7). The interstack coupling between TTF and CA parallel to the (**b**,**c**) plane is achieved by the clearly bent hydrogen bonds shown in Fig. 6, which become really active only in the low-temperature phase. Although their angular geometry is almost not affected and maintains a quite important deviation from linearity, they present a significant shortening until their O $\cdots$ H distances become shorter than the critical value of 2.4 Å. In addition to S $\cdots$ Cℓ contacts, the interstack connection parallel to the (**a**,**b**) plane between TTF and CA molecules $\mathbf{a}/2+\mathbf{b}$ apart, is assured by the quasilinear H bonds shown in Fig. 7. Thus, for both types of hydrogen bonding in the ionic phase, a clear enhancement of the bond strength of three-dimensional character is directly measurable from the distances between the involved oxygen and hydrogen atoms. Due to this fact, and also to the other closest contacts discussed above, an enhancement of the rigidity of the system can be expected in the ionic phase, in addition to the normal thermal effect at low temperatures. This could lead to some increase of phonon frequencies, and, more specifically, to a small hardening of the elastic constants of the material.

C. Intramolecular deformation

Figure 8 displays the intramolecular geometry of the TTF and the CA molecules at the different experimental

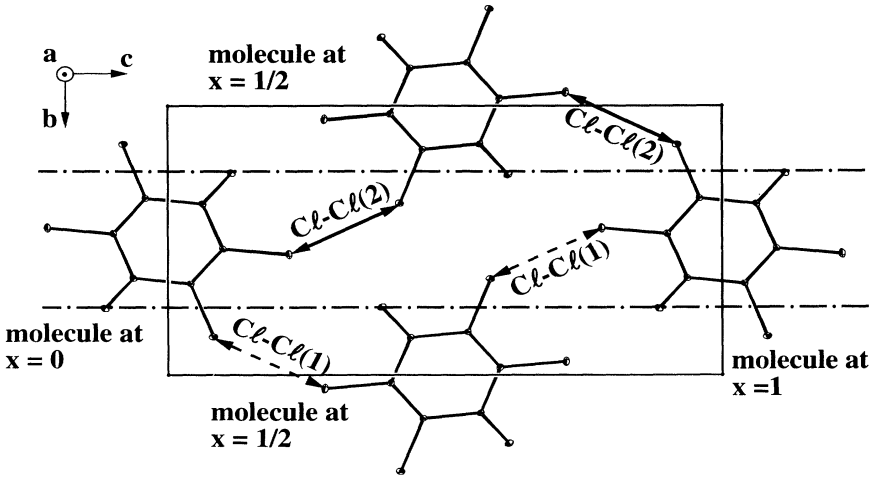

FIG. 5. The closest intermolecular Cℓ-Cℓ contacts.

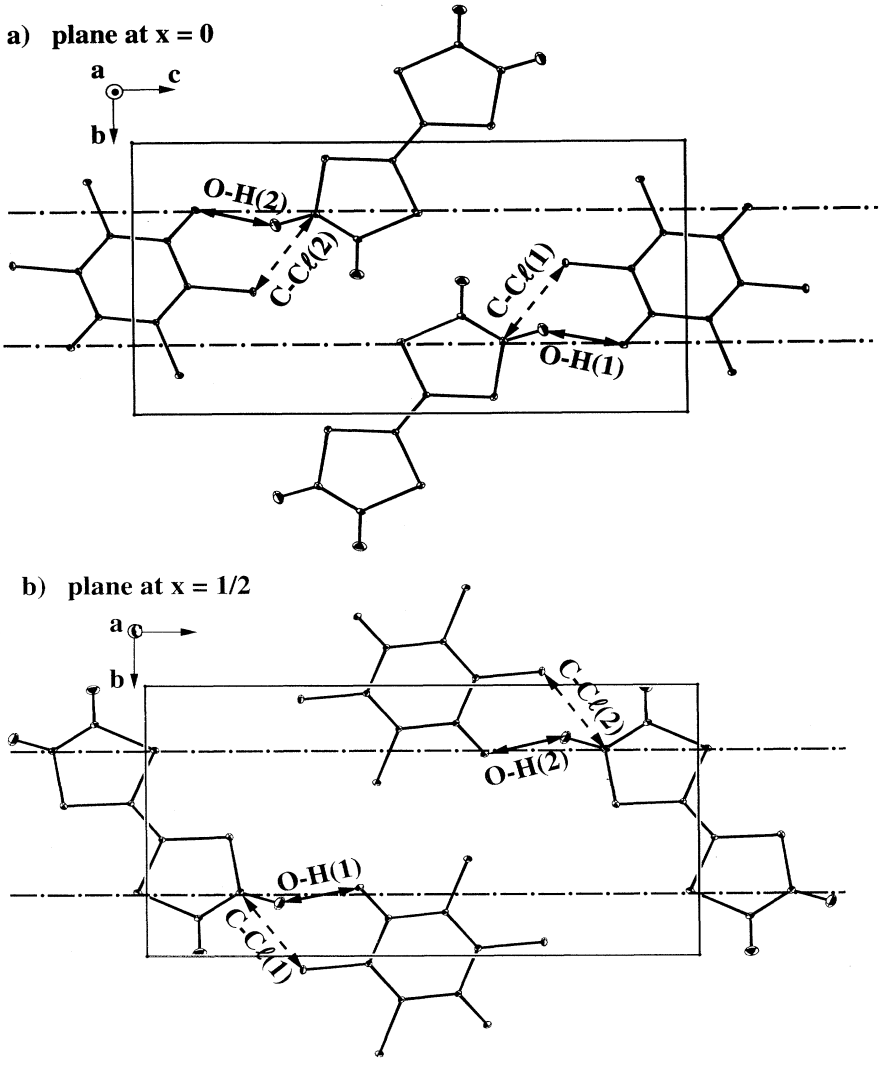

FIG. 6. Interstack C-Cℓ (— — —) and O-H (——) interactions projected onto the (**b**,**c**) plane at: (a) **x**=0, (b) **x**=$\frac{1}{2}$.

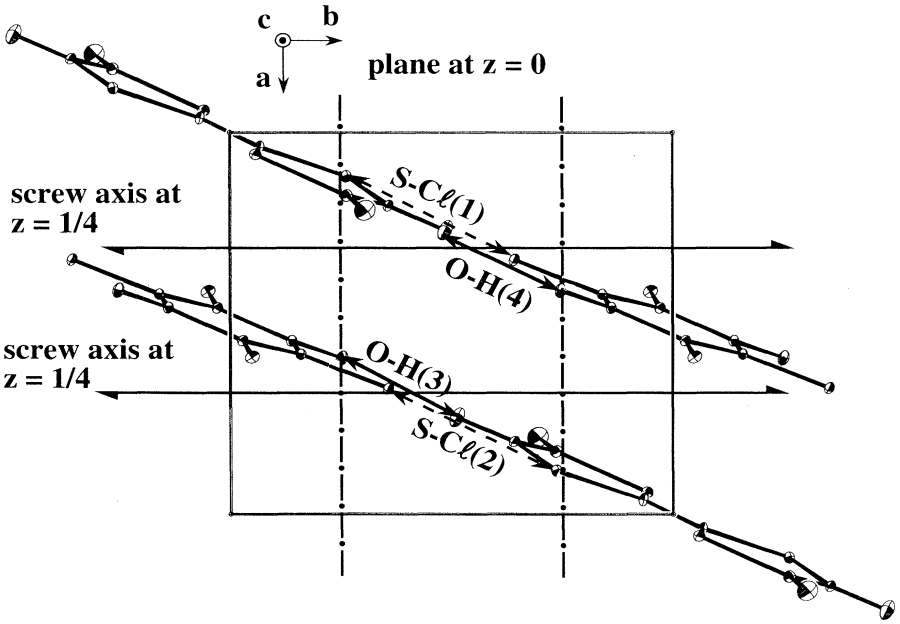

FIG. 7. Interstack S-Cℓ (— — —) and O-H (——) interactions projected onto the (**a**,**b**) plane.

TABLE V. C-H · · · O hydrogen bonds: evolution with temperature. Symmetry equivalent values are given in curly brackets. Distances shorter than the sum of van der Waals radii are marked by an asterisk *.

		X rays (Ref. 23)	Neutrons, this work				
		300 K	300 K	90 K_{TC}	90 K	40 K_{TC}	40 K
O-H (Å)							
	(1)	{2.62}	{2.490(5)}	{2.442(8)}	{2.410(3)}	{2.436(8)}	2.359(3)*
	(2)						2.297(2)*
	(3)	{2.62}	{2.343(5)}*	{2.275(8)}*	{2.273(3)}*	{2.256(8)}*	2.219(2)*
	(4)						2.188(2)*
C-O (Å)							
	(1)	{3.364}	{3.355(2)}	{3.302(5)}	{3.277(2)}	{3.293(5)}	3.216(1)
	(2)						3.212(1)
	(3)	{3.444}	{3.433(3)}	{3.366(6)}	{3.347(2)}	{3.348(6)}	3.311(1)
	(4)						3.271(1)
C-H · · · O (°)							
	(1)	{143}	{135.3(3)}	{134.6(6)}	{136.0(3)}	{134.5(6)}	135.3(2)
	(2)						139.5(1)
	(3)	{178}	{172.2(3)}	{173.1(6)}	{173.1(2)}	{173.2(6)}	167.2(2)
	(4)						178.0(1)

temperatures. Neutron diffraction, due to its relative scattering cross sections, yields precise hydrogen positions and thus a well-defined geometry of the complete TTF molecules. At 300 K, except for C-H bonds, the intramolecular distances and angles of both molecules obtained by neutron scattering, are in good agreement with those from the x-ray structure analysis.[25]

Whereas temperature decrease to 90 K alters strongly the **a** cell parameter, i.e., the stacking direction (the contraction is about 3% along this direction while it is only about 0.5% along **b** and **c**), the intramolecular geometry is only weakly affected by such important compression of the electron-donor TTF and electron-acceptor CA molecular orbitals. Both types of molecules stay planar as can be directly seen from the side projections of Fig. 8. Besides, the values of the anisotropic thermal parameters remain normal at the approach of the phase transition, although well pronounced pretransitional phenomena were unambiguously detected in the neutral phase by dielectric measurements,[22] $^{35}C\ell$ NQR spectroscopy[21,23] and IR spectroscopy.[34] This "nonobservation" is certainly caused by the small displacements involved in the dimerization process and also by the clear first-order character of the transition.

In the ionic phase at 40 K, the intramolecular geometry is clearly different. In particular, a loss of inversion symmetry is obvious for both the TTF and the CA molecules: most of the high-temperature equivalent bond lengths become significantly different in the ionic phase. The part of the TTF molecule formed by atoms 1–7 has 1–2 % longer bond distances than the other one formed by atoms 8–14 (the standard deviations are of 0.1–0.2 %). This part of the TTF molecule (atoms 1–7) is also less inclined with respect to the CA molecule of the dimer, as can be obtained from the dihedral angles between least-square planes of, respectively, the two moieties of the TTF molecule and of the CA molecule: at 300 and 90 K, the TTF(1–7)-CA and TTF(8–14)-CA angles are equivalent by symmetry; they change from 2.44° to 2.08° with decreasing temperature; at 40 K, both parts of the TTF molecule are independent and the TTF(1–7)-CA angle (2.35°) becomes significantly smaller than the TTF(8–14)-CA one (3.23°). These features in conjunction with the displacement in opposite directions along **b** of both components of the dimer (see Table III) have as consequence an enhancement of the molecular orbital overlap between donor and acceptor molecules, and thus stabilize the dimeric arrangement. The CA molecule is slightly bent with only non ring bonds clearly affected, i.e., C=O and C-Cℓ. These geometry modifications explain both the frequency shift of the $^{35}C\ell$ NQR lines and their splitting observed at the transition.[21,23] Due to the limited resolution, only three NQR lines could be observed on powder samples, one of them having twice the intensity of the others. Indeed, we see that among the four nonequivalent Cℓ sites in the ionic phase, two have very similar intramolecular environment. The complete splitting of the nonresolved NQR line was achieved recently on single crystals, thanks to the better homogeneity of the electric-field gradient.[42]

One can expect to extract information on the change of the charge transfer between the TTF and the CA molecules from the evolution of the internal molecular geometry. As already developed for low-dimensional organic complexes,[43–45] an estimate of the degree of charge transfer can be obtained via empirical formulas implying the ratio (estimate q_1) or the difference (estimate q_2) between the central C=C and the averaged adjacent C-S bond lengths of the TTF molecule, r and s, respectively. In this way, from a collection of structural data concerning a series of organic salts containing TTF molecules, Umland *et al.*[45] have set up the following formulas for an estimate of charge transfer: $q_1 = -15.55 + 20.42\ r/s$ and $q_2 = 4.49 + 10.748\ (r - s)$, the former being considered as more reliable. From these two estimates, the degree of charge transfer of TTF-CA evolutes from 0.4 at 300 K,

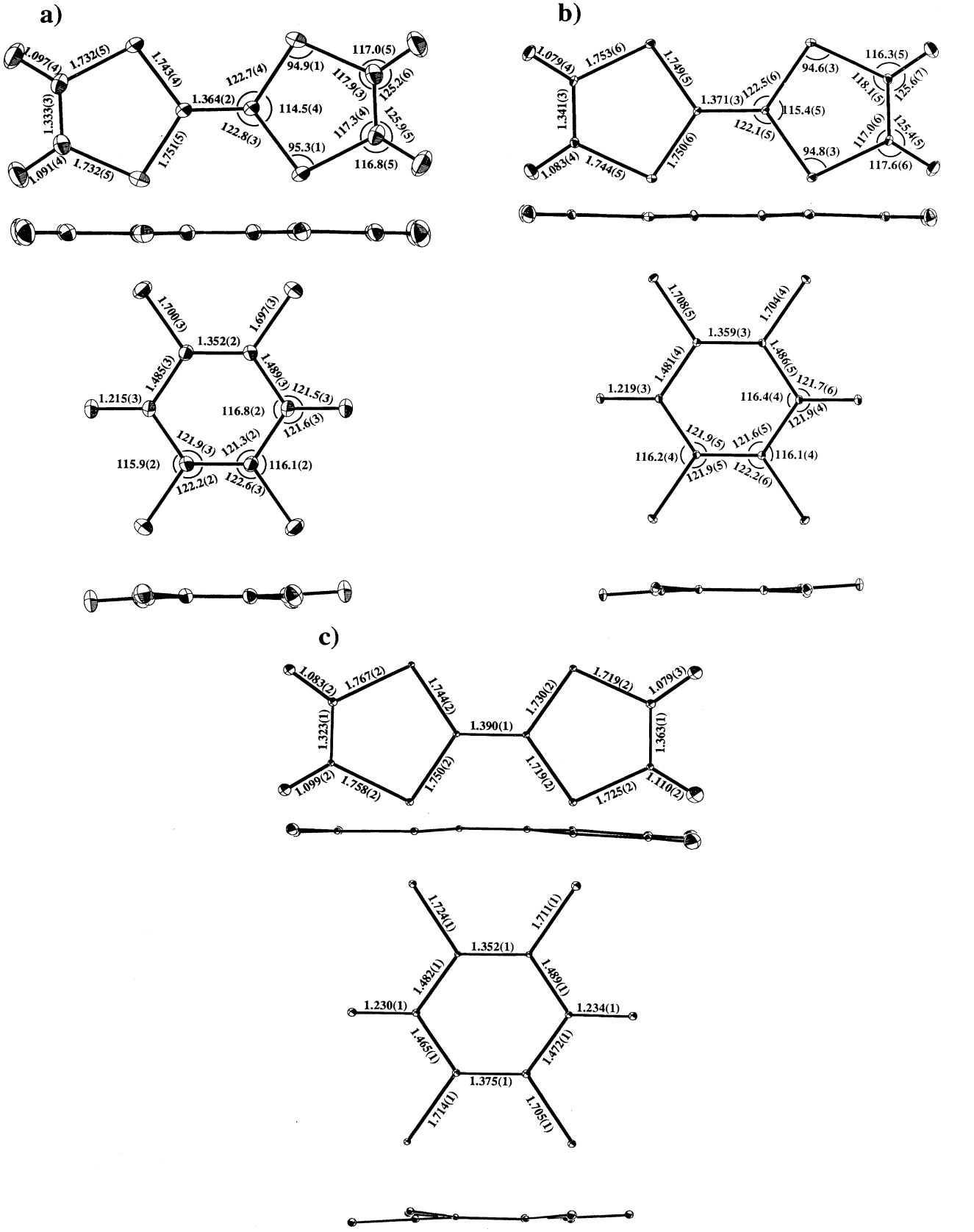

FIG. 8. Intramolecular geometry at the different temperatures (a) 300 K, (b) 90 K, (c) 40 K (the bonding angles can be determined from the atomic coordinates).

0.5 (q_1) or 0.4 (q_2) at 90 K in the N phase to 0.8 at 40 K in the I phase. As mentioned,[45] this method indicates only a tendency, in particular because the degree of charge transfer of the compiled organic salts has not always been determined precisely. In spite of the fact that values larger than those deduced from the temperature-dependent charge-transfer absorption band[11] or from intramolecular infrared active vibration[12] were obtained, it is very satisfying to note that the evolution of ρ is well reproduced: the weak increase reported just above the transition is confirmed and a charge-transfer variation of 0.4 is found.

V. CONCLUSION

The results presented in this paper provide fundamental new insight into the structural properties that are coupled with the electronic aspect of the neutral-to-ionic phase transition of TTF-CA. A B_u symmetry order parameter, associated with the creation of ferroelectric chains of (TTF-CA) dimers, governs the instability with a direct translation equivalent group-subgroup relation between the involved space groups. In the low-temperature phase, dipole moments appear with a ferroelectric spatial arrangement giving rise to weak long-range order dipolar interactions. Application of neutron-diffraction techniques was essential to overcome the intrinsic difficulties that the details of this phase transition impose, in particular due to the specific symmetry of the problem (dimerization mainly along the **a** direction and superstructure reflections sensitive to the atomic displacement component along the **b** direction). The evolution of the order parameter was carefully analyzed on triple-axis spectrometer before solving the crystal structures from data obtained on a four-circle diffractometer. In this way, we were able to prove that the normally accepted van der Waals contacts between the molecules are significantly compressed to form, first of all, the dimers but also to some extent, a three-dimensional network that includes all molecules. Moreover, taking into account compilations on other charge-transfer crystals containing TTF molecules, it has been possible to extract the degree of charge transfer in a satisfying way from the evolution of the averaged intramolecular geometry. On the other hand, the effect of the ferroelectric order parameter on the intramolecular geometry of both the TTF and the CA molecules was clearly evidenced from the loss of centrosymmetry in agreement with $^{35}C\ell$ NQR results. Further structural results on the pressure effects and on the hysteresis phenomena around $T_{N\text{-}I}$ will be presented in two following papers.

ACKNOWLEDGMENTS

The authors want to thank J. L. Baudour, Y. Délugeard, C. Koenig, J. Lajzerowicz, T. Luty, and J. P. Pouget for fruitful discussions.

*Present address: Institut für Kristallographie, Rheinisch Westfälische Technische Hochschule, Jägerstraße 17-19, D-52066 Aachen, Germany.

†Present address: Kernforschungszentrum Karlsruhe, Institut für Nukleare Festkörperphysik, D-76021 Karlsruhe, Germany.

‡Present address: IBM Halbleiter GmbH, D-71034 Böblingen-Hulb, Germany.

[1]J. B. Torrance, J. E. Vazquez, J. J. Mayerle, and V. Y. Lee, Phys. Rev. Lett. **46**, 253 (1981).

[2]J. B. Torrance, Mol. Cryst. Liq. Cryst. **126**, 55 (1985).

[3]J. B. Torrance, A. Girlando, J. J. Mayerle, J. I. Crowley, V. Y. Lee, P. Batail, and S. J. La Placa, Phys. Rev. Lett. **47**, 1747 (1981).

[4]Z. G. Soos and S. Mazumdar, Phys. Rev. B **18**, 1991 (1978).

[5]Z. G. Soos, L. R. Ducasse, and R. M. Metzger, J. Phys. Chem. **77**, 3036 (1982).

[6]B. Horovitz and B. Schaub, Phys. Rev. Lett. **50**, 1942 (1983).

[7]N. Nagaosa and J. I. Takimoto, J. Phys. Soc. Jpn. **55**, 2735 (1986); **55**, 2745 (1986).

[8]N. Nagaosa, J. Phys. Soc. Jpn. **55**, 2754 (1986); **55**, 3488 (1986).

[9]T. Luty, J. Chem. Phys. **87**, 3137 (1987).

[10]T. Luty and B. Kuchta, Phys. Rev. B **35**, 8542 (1987).

[11]C. S. Jacobsen and J. B. Torrance, J. Chem. Phys. **78**, 112 (1983).

[12]A. Girlando, F. Marzola, C. Pecile, and J. B. Torrance, J. Chem. Phys. **79**, 1075 (1983).

[13]T. Mitani, G. Saito, Y. Tokura, and T. Koda, Phys. Rev. Lett. **53**, 842 (1984).

[14]K. Takaoka, Y. Kaneko, H. Okamoto, Y. Tokura, T. Koda, T. Mitani, and G. Saito, Phys. Rev. B **36**, 3884 (1987).

[15]N. Nagaosa, Solid State Commun. **57**, 179 (1986).

[16]B. Horovitz and J. Solyom, Phys. Rev. B **35**, 7081 (1987).

[17]Y. Tokura, S. Koshihara, Y. Iwasa, H. Okamoto, T. Komatsu, T. Koda, N. Iwasawa, and G. Saito, Phys. Rev. Lett. **63**, 2405 (1989).

[18]K. Kikuchi, K. Yakushi, and H. Kuroda, Solid State Commun. **44**, 151 (1982).

[19]H. Bartholin, J. L. Baudour, C. Breandon, R. Tchapoutian, H. Cailleau, and D. Perrin, Solid State Commun. **63**, 223 (1987).

[20]M. H. Lemée-Cailleau, B. Toudic, H. Cailleau, F. Moussa, M. Le Cointe, G. Silly, and N. Karl, Ferroelectrics **127**, 19 (1992).

[21]J. Gallier, B. Toudic, Y. Délugeard, H. Cailleau, M. Gourdji, A. Péneau, and L. Guibé, Phys. Rev. B **47**, 11 688 (1993).

[22]H. Okamoto, T. Mitani, Y. Tokura, S. Koshihara, T. Komatsu, Y. Iwasa, T. Koda, and G. Saito, Phys. Rev. B **43**, 8224 (1991).

[23]M. Gourdji, L. Guibé, A. Péneau, J. Gallier, B. Toudic, and H. Cailleau, Z. Naturforsch. **47a**, 257 (1991).

[24]C. Ayache and J. B. Torrance, Solid State Commun. **47**, 789 (1983).

[25]J. J. Mayerle, J. B. Torrance, and J. I. Crowley, Acta Crystallogr. B **35**, 2988 (1979).

[26]Y. Kanai, M. Tani, S. Kagoshima, Y. Tokura, and T. Koda, Synth. Met. **10**, 157 (1984/85).

[27]S. Kagoshima, Y. Kanai, M. Tani, Y. Tokura, and T. Koda, Mol. Cryst. Liq. Cryst. **120**, 9 (1985).
[28]T. Luty, J. Phys. Soc. Jpn. **61**, 3636 (1992).
[29]P. Batail, S. J. La Placa, J. J. Mayerle, and J. B. Torrance, J. Am. Chem. Soc. **103**, 951 (1981).
[30]B. I. Swanson, M. A. Stroud, S. D. Conradson, and M. H. Zietlow, Solid State Commun. **65**(11), 1405 (1988).
[31]N. Karl, in *Materials for Non-Linear and Electro-Optics,* edited by M. H. Lyons, IOP Conf. Proc. No. 103 (Institute of Physics, Bristol, 1989), p.107.
[32]Y. Yoshinari, Y. Maniwa, T. Takahashi, K. Mizoguchi, and T. Mitani, Synth. Met. **19**, 521 (1987).
[33]B. Toudic, J. Gallier, M. Boumaza, and H. Cailleau, J. Phys. (Paris) **51**, 1671 (1990).
[34]A. Moréac, A. Girard, Y. Marqueton, and Y. Délugeard (unpublished).
[35]Reliability factor $R=\sum\|F_0-|F_c|\|/\Sigma F_0$ weighted reliability factor $R_w=[\Sigma w(F_0-|F_c|)^2/\Sigma wF_0^2]^{1/2}$, weighting scheme $w(F)=1/\sigma^2(F)$, goodness of fit GDF$=[\Sigma w(F_0-|F_c|)^2/(m-n)]^{1/2}$, m: number of independent reflections with $F_0>2.5\sigma(F_0)$, n: number of independent parameters to refine.
[36]J. Lajzerowicz and J. F. Legrand, Phys. Rev. B **17**, 1438 (1978).
[37](a) L. Pauling, *The Nature of Chemical Bond* (Cornell University Press, Ithaca, New York, 1960); C-C: 3.4–3.7 Å, C-Cℓ: 3.5–3.65 Å, S-C: 3.55–3.70 Å, S-Cℓ: 3.65 Å, O-H: 2.4–2.8 Å; Cℓ-Cℓ: 3.6 Å; C-O: 3.1–3.25 Å. (b) W. H. Baur, Acta Crystallogr. B **28**, 1456 (1972).
[38]R. Taylor and O. Kennard, J. Am. Chem. Soc. **104**, 5063 (1982).
[39]G. R. Desiraju and K. V. Radhakishan, J. Am. Chem. Soc. **111**, 4838 (1989).
[40]I. Olovsson and P. G. Jönsson, *The Hydrogen Bond Recent Developments in Theory and Experiments,* edited by P. Schuster *et al.* (North-Holland, Amsterdam, 1976).
[41]D. J. Sutor, J. Chem. Soc. 1105 (1963).
[42]M. Le Cointe, J. Gallier, H. Cailleau, M. Gourdji, A. Péneau, and L. Guibé, Solid State Commun. (to be published); M. Le Cointe, Ph.D. thesis, University of Rennes 1, 1994.
[43]S. Flandrois and D. Chasseau, Acta Crystallogr. B **33**, 2744 (1977).
[44]A. Girlando, C. Pecile, and J. B. Torrance, Solid State Commun. **54**, 753 (1985).
[45]T. C. Umland, S. Allie, T. Kuhlmann, and P. Coppens, J. Phys. Chem. **92**, 6456 (1988).